A Control Framework for Ocean Wave Energy Conversion Systems: The Potential of Moments

A Control Framework for Ocean Wave Energy Conversion Systems: The Potential of Moments

Article *in* Annual Review of Control Robotics and Autonomous Systems · November 2023

DOI: 10.1146/annurev-control-070523-115155

2 authors:

Nicolás Faedo
Politecnico di Torino
107 PUBLICATIONS **1,294** CITATIONS
SEE PROFILE

John Ringwood
Maynooth University
506 PUBLICATIONS **10,221** CITATIONS
SEE PROFILE

ANNUAL REVIEWS

Annual Review of Control, Robotics, and Autonomous Systems

A Control Framework for Ocean Wave Energy Conversion Systems: The Potential of Moments

Nicolás Faedo[1] and John V. Ringwood[2]

[1]Marine Offshore Renewable Energy Lab, Department of Mechanical and Aerospace Engineering, Politecnico di Torino, Turin, Italy; email: nicolas.faedo@polito.it

[2]Centre for Ocean Energy Research, Department of Electronic Engineering, Maynooth University, Maynooth, Ireland; email: john.ringwood@mu.ie

Annu. Rev. Control Robot. Auton. Syst. 2024. 7:5.1–5.26

The *Annual Review of Control, Robotics, and Autonomous Systems* is online at control.annualreviews.org

https://doi.org/10.1146/annurev-control-070523-115155

Keywords

wave energy, model reduction, energy-maximizing control, moments, wave energy arrays

Abstract

The control of wave energy converters (WECs) to maximize power capture is a challenging problem. In particular, the nature of the wave excitation, which is in general panchromatic (or multi-sinusoidal), presents a reciprocating energy source that needs to be rectified through some means. In addition, the development of suitable control-oriented models is also challenging, requiring correct representation of system hydrodynamics and power take-off (PTO) components, while also lending themselves to control synthesis and real-time computational performance, along with a challenging optimal control problem. This article presents a moment-based mathematical framework for the formulation and solution of WEC control. It shows that moments are ideally suited to WEC control in terms of their ability to accurately characterize the nature of the wave excitation force (and the consequent evolutions in the system variables) while also gracefully including hydrodynamic and PTO nonlinearities as well as a natural extension to WEC arrays. Model reduction, to mold the system model into a control-friendly form, is also a feature of this framework.

1. INTRODUCTION

Wave energy converter (WEC) prototypes come in a wide variety of shapes and sizes and utilize a variety of operating principles (2). While this makes it challenging to identify a generic case, the common goal is to maximize harvested energy for a given capital and operational expenditure. Effective control of WECs has been identified as a key challenge in mitigating climate change (3), and various approaches to WEC control have evolved over the past half century (4). In addition to the variety of prototypes and principles, the generality of the WEC control problem demands a comprehensive toolset—able to deal with both linear and nonlinear system representations and extensible to multibody, multi-degree-of-freedom (multi-DOF), and multi-WEC cases—while maintaining the possibility for real-time implementation. In addition, the construction of a full system mathematical model, suitable for control synthesis, is not an insignificant step, nor is the customization of models to make them tractable, both analytically and computationally, for control design.

Early WEC controllers, in essence, exploited the maximum power transfer theorem (5), where ocean waves are assumed to be monochromatic, or a predominant single (monochromatic) frequency can be identified within a panchromatic sea spectrum. Such controllers could be extended to WEC arrays but could not effectively handle panchromatic (realistic) ocean waves or system physical constraints (force, displacement, etc.), nor could they be extended to the nonlinear case. Crucially, for many WEC types, the action of control itself serves to broaden the operational space and excite significant hydrodynamic nonlinearities (6).

Contemporary WEC controllers, beginning in 2010 (7), adopted an approach based on model predictive control (8), though with a bilinear power objective rather than the usual quadratic terms. This gave the potential to effectively handle system constraints, and the predictive framework could incorporate estimation and forecasting of the wave excitation force, now required in the solution of the panchromatic WEC control problem. However, the bilinear cost term needs to be regularized by suitable quadratic terms to convexify the optimization problem, and the incorporation of a nonlinear model further accentuated the issue. Also, the zero-order-hold representations are a relatively poor fit for the continuously changing but smooth signals associated with ocean waves, with relatively short sampling periods heightening computational demand. A potential solution was provided by Cretel et al. (9), who utilized a first-order hold, also alleviating the convexity issue, albeit with realization issues. However, a variety of recent techniques using various basis function representations, falling into the category of spectral/pseudospectral methods, have shown promise (4, 8) and can, in fact, be shown to be a subset of the framework presented here.

This article[1] presents a moment-based mathematical framework for the solution of the WEC and WEC array control problem, with the following advantages:

1. The fundamental nature of the system signals can be specified by a signal generator, chosen to be multiharmonic, that provides a good match with ocean and ocean-derived system signals.
2. Mainly as a result of the first advantage, the analysis focuses exclusively on the steady-state behavior of the system, with no effort expended on the system transient response, which is of little interest for this application.

[1]A preliminary version of this review was presented in a conference paper (1); the present article significantly extends that paper by providing a detailed account of each of the elements within the framework, starting from the theoretical background and including experimental implementation of moment-based control for WEC systems.

3. The moment-based WEC control techniques, initially developed for linear WEC models, can be extended to cover hydrodynamic and power take-off (PTO) nonlinearities.
4. The methods can be seamlessly extended to cover multibody, multi-DOF, and multi-WEC cases, with an increase in the dimension of the representation.
5. Moment-based analysis was initially popularized in the control community as a model reduction tool (10), facilitating the customization of WEC models for control synthesis and providing a mechanism to achieve a trade-off between objective fidelity and computational complexity for specific WEC cases.
6. Moment-based controllers have been robustified to cater to uncertainty in both the system model and excitation force estimates (see Section 5.4).
7. A set of efficient mathematical tools are available to solve the optimization problems arising from the moment-based representation, and real-time WEC control has been demonstrated for both single WECs and arrays of WECs (see Section 6).

In this review, $\mathbb{R}^+$ denotes the set of nonnegative real values, while $\mathbb{C}^0$ denotes the sets of complex values with zero real part. If $x \in \mathbb{C}^n$, then the notation $x_j \in \mathbb{C}$ denotes the jth entry of x. The notation $\lambda(A)$, with $A \in \mathbb{C}^{n\times n}$, is used for the set of eigenvalues of A. The notation $\mathbb{N}_K$ is used for the set of natural numbers up to K, i.e., $\mathbb{N}_K = \{1, \ldots, K\} \subset \mathbb{N}$. The symbol $\otimes$ is used for the standard Kronecker product. The notation $\mathbb{I}$ is used for the identity matrix, where the dimensions are always clear from the context. The direct sum of N matrices $A_i \in \mathbb{R}^{n\times n}$ is denoted as $\bigoplus_{i=1}^{N} A_i = \text{diag}(A_1, \ldots, A_N) \in \mathbb{R}^{nN\times nN}$.

2. AN OVERVIEW OF THE FRAMEWORK

Figure 1 provides an overview of the moment-based control design framework presented in this article, which highlights both the specific approach taken in this framework to achieve energy-maximizing moment-based control solutions and alternative paths to those described in this article. For instance, one alternative path involves the use of moment-based linear model reduction to generate linear control-oriented models that are suitable for a wide range of optimal control procedures, based on user preference and experience (e.g., the techniques mentioned in Section 1).

In general, as can be appreciated from **Figure 1**, the framework is comprehensive, guiding the user from the initial modeling stage to the experimental implementation of control strategies. If the ultimate objective is that of control design and synthesis, a primary goal is to transform the system model into a suitable form for model-based control and estimation procedures. While data-driven or data-based models can often be parameterized to meet the requirements of model-based WEC control design (informing the modeling stage with respect to the main requirements for control-oriented applications), physics-based models for hydrodynamics and PTO components seldom do so, particularly in the case of the former, due to the intrinsic complexity behind hydrodynamic modeling (see also the discussion in Section 3.1). Therefore, some form of model manipulation or reduction is virtually always necessary. Within the moment-based framework, both linear and nonlinear model reduction techniques have been developed to refine the models for WEC control design purposes, as discussed at length in Section 4.

On the control design front, the framework encompasses linear and nonlinear WEC control design, array control design, and robust control design to account for modeling uncertainty, always in line with the ultimate aim of practical implementation. These designs are discussed explicitly in Section 5, and an overview of an experimental application on a WEC prototype (in both stand-alone and array configurations) is provided in Section 6. For the case of estimation of wave excitation forces, which are required as inputs for optimal noncausal WEC control schemes (see

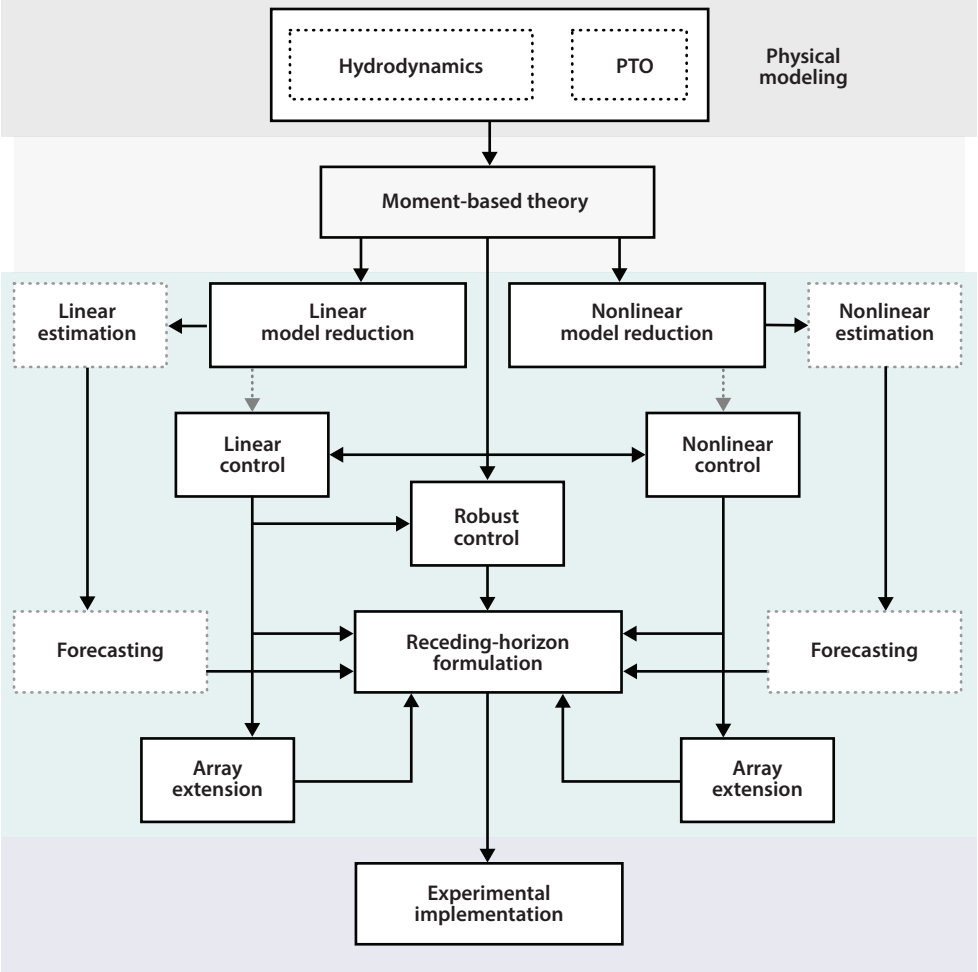

Figure 1

Overview of the moment-based framework for WECs, from the initial modeling stage (*top*) to the experimental implementation of control strategies (*bottom*). Solid black arrows show the specific approach taken in this framework to achieve energy-maximizing moment-based control solutions, and dotted gray arrows show alternative paths that are also possible; solid rectangles indicate components that are included or discussed within the presented framework, while dotted rectangles are alternative options that can be included by exploiting tools from the framework but are not specifically addressed in this review. Abbreviations: PTO, power take-off; WEC, wave energy converter. Figure adapted with permission from Reference 1.

Section 5) in both single devices and arrays, we direct readers to References 11 and 12, respectively. We do note that the development of moment-based estimators and forecasters is an ongoing research topic, with some progress reported in Reference 13.

3. PRELIMINARIES

This section briefly introduces both the fundamentals of control-oriented WEC modeling (Section 3.1) and the main elements of moment-based theory (Section 3.2) as applied to WEC systems. Additional references are provided where appropriate for further detailed exploration by interested readers.

3.1. Fundamentals of Control-Oriented Wave Energy Converter Modeling

The underlying modeling framework for a generic WEC system has its origins in the well-known Navier–Stokes equations, which essentially define the dynamics of fluid–structure interactions in both space and time. The nature of these equations is intrinsically complex, virtually always necessitating sophisticated numerical schemes for computing approximate solutions of practical value. Due to this underlying complexity and the computational burden associated with high-fidelity numerical approximations, a set of assumptions are commonly employed within the literature when deriving control-oriented models for WEC systems, forming potential flow theory (14). In particular, if we consider a generic body geometry in water waves, the main modeling assumptions (MAs) characterizing linear potential flow theory are that (*a*) the flow is frictionless (inviscid) and irrotational (MA1), (*b*) the amplitude of the body motion is significantly smaller than its dimension (MA2), and (*c*) linear wave theory (as described in, e.g., Reference 15) holds (MA3).

These three assumptions (MA1–3), together with an associated set of boundary conditions (14), give origin to a family of efficient numerical techniques known as boundary element methods (BEMs), which provide approximate solutions to the Navier–Stokes equations under linear potential flow conditions. BEMs are popular within the WEC literature, particularly in control- and estimation-oriented studies, with researchers exploiting several established BEM codes, both open source (e.g., 16) and commercial (e.g., 17).

Linear potential flow theory, leveraging BEM techniques, gives origin to the most widely used operator in control-oriented modeling for WECs: the so-called Cummins equation (18). Consider, for simplicity, a WEC system moving in a single DOF.[2] Following linear potential flow theory, the equation of motion can be written, for $t \in \mathbb{R}^+$, as

$$m\ddot{z} = f_e + f_r + f_{re} - f_u, \qquad 1.$$

where $m \in \mathbb{R}$ is the mass (or, alternatively, inertia) of the device, $z(t) \in \mathbb{R}$ denotes the displacement of the floating body, $f_e(t) \in \mathbb{R}$ is the wave excitation force, $f_r(t) \in \mathbb{R}$ is the radiation force, $f_{re}(t) \in \mathbb{R}$ is the hydrostatic restoring force, and $f_u(t) \in \mathbb{R}$ represents the control input, exerted via an associated PTO system.

The wave excitation f_e is essentially the force exerted on the device by the action of the surrounding wave field. Though f_e can be considered a disturbance (i.e., an uncontrollable input) to the WEC system, it plays a fundamental role in the device energy extraction process, being the direct link to the wave energy source. The radiation force f_r is defined as the hydrodynamic force acting on the body due to the fluid itself, in the absence of incident waves, and can be written in terms of the following convolution operator:

$$f_r = -m_\infty \ddot{z} - \dot{z} * k_r, \qquad 2.$$

in which $k_r(t) \in \mathbb{R}$ is the (causal) radiation impulse response function, and $m_\infty \in \mathbb{R}$ is the so-called added-mass infinite-frequency asymptote (see, e.g., 5).

Remark 1. Though the map k_r in Equation 2 defines an associated linear time-invariant system, the numerical computation of such an impulse response is performed in a nonparametric form, using BEM codes, and hence only a finite set of points (in either the time or frequency domain) is available (see, e.g., 20). The associated lack of a closed-form solution effectively represents an issue, particularly from a computational perspective. Section 4 explicitly addresses this issue using moment-based theory.

The restoring force f_{re} is defined as the force arising from the balance of gravitational and buoyancy forces, which, within linear potential flow theory assumptions, can be written in closed

[2] An analogous procedure can be followed for WEC systems moving in N DOFs (see, e.g., 19).

form as

$$f_{\mathrm{re}} = -s_{\mathrm{h}} z, \tag{3.}$$

where $s_{\mathrm{h}} \in \mathbb{R}$ is referred to as the restoring coefficient. Finally, f_{u} is the control input applied via the corresponding PTO system on the WEC device. This input is to be designed in such a way that maximum energy absorption from the incoming wave field is achieved, ideally in every possible operating condition, hence significantly improving the overall performance of the WEC system. The specific computation of f_{u} is performed in terms of an associated optimal control problem (OCP), which Section 5 formally describes and solves by leveraging moment-based theory. With the forces described above, Equation 1 can be written in terms of the following WEC dynamical system $\mathcal{G}$:

$$\mathcal{G} : \begin{cases} \ddot{z} & = \bar{M}\left(-\dot{z} * k_{\mathrm{r}} - s_{\mathrm{h}} z + f_{\mathrm{e}} - f_{\mathrm{u}}\right), \quad y = \dot{z} = v, \end{cases} \tag{4.}$$

where $\bar{M} = M^{-1}$, with $M = m + m_{\infty}$, and, without any loss of generality, the output y is set to be the velocity vector associated with the motion of the device $\dot{z}$, in line with the energy-maximizing OCP for WECs, as defined in Section 5.

As discussed at the beginning of this section, the operator in Equation 4 is derived by exploiting linear potential flow theory assumptions. Since the energy-maximizing nature of the control solution itself tends to require large device motion (displacement or velocity), the set of hypotheses adopted for linear modeling can lead to nonrepresentative dynamical models. In particular, under controlled conditions, MA2 can be potentially violated by the action of f_{u}. This phenomenon, known in the field as the WEC control paradox, is discussed at length in Reference 6. In an effort to broaden the scope of application of Cummins's formulation and alleviate the overall impact of this control paradox, a common practice is to append a number of relevant additional forces affecting the WEC system via relatively simple (though typically nonlinear) analytical representations.

The most common source of nonlinearity included in Equation 4 stems from viscous drag effects. This particular phenomenon, which can be attributed mainly to shear stress, is commonly added in terms of a C^{∞} Morison-like equation (21). Nonlinear restoring forces are also often included, better able to represent WECs with a nonconstant cross-sectional profile. Given the nature of the restoring phenomenon (which is linked to the static Froude–Krylov force; see, e.g., 22), polynomial parameterizations in z are commonly employed (see, e.g., 23). Finally, recent control-oriented studies (see, e.g., 24, 25) also include mooring forces as part of dynamical WEC descriptions, effectively recognizing the relevance of these effects on the overall system response. Adopted closed-form expressions for mooring forces are often based on polynomial representations, inspired by early results within the more general field of ocean engineering (see, e.g., 26, 27).

We summarize the extensions to the linear Cummins formulation in Equation 4, discussed immediately above, by means of a general (sufficiently smooth) nonlinear map f_{nl}, i.e.,

$$\mathcal{G} : \begin{cases} \ddot{z} = \bar{M}\left(-\dot{z} * k_{\mathrm{r}} - s_{\mathrm{h}} z + f_{\mathrm{e}} - f_{\mathrm{u}} + f_{\mathrm{nl}}\right), \quad y = \dot{z} = v. \end{cases} \tag{5.}$$

An overall schematic diagram of the dynamical Equation 5 can be appreciated in **Figure 2**, where the device considered, for illustration purposes, is the so-called Wavestar system (see Section 6). Furthermore, with an appropriate choice of state variables (i.e., $x = [z,\ \dot{z}]^{\mathrm{T}}$), Equation 4 can be written in terms of a corresponding state-space representation,

$$\mathcal{G} : \begin{cases} \dot{x} = g(x, f_{\mathrm{e}} - f_{\mathrm{u}}), \quad y = Cx, \end{cases} \tag{6.}$$

where the map g and corresponding output matrix C can be derived from Equation 5.

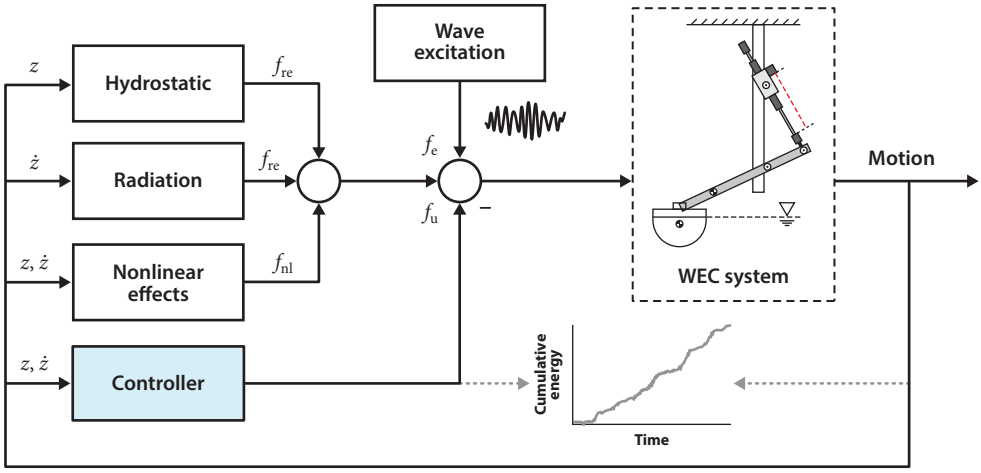

Figure 2

Schematic representation of the WEC dynamical equation. Note that cumulative converted energy is optionally calculated by integrating the product of the control (PTO) force and the device velocity, indicated by the dotted gray arrows. Abbreviations: PTO, power take-off; WEC, wave energy converter.

Remark 2. Following standard physical principles, it is possible to show that the zero equilibrium of $\dot{x} = g(x, 0)$ in Equation 6 is locally exponentially stable for any physically meaningful map g. For further discussion, we direct interested readers to, e.g., Reference 28.

3.2. Fundamentals of Moment-Based Theory for Wave Energy Converter Systems

Following the main modeling elements introduced in Section 3.1, we present a brief account of the system-theoretic interpretation of moment-based theory for WEC systems (based on the seminal work presented in Reference 10) and the first relevant application in the field (based on work presented in Reference 29). The theoretical framework in Reference 10 and the associated definition of a moment were originally exploited to produce reduced-order models for a large class of dynamical systems in diverse operating (input) conditions (see Reference 30 and the review presented in Reference 31). Reference 29 is, to the best of our knowledge, the first application of moments that departs from the original model reduction objective, in which the framework in Reference 10 is exploited to transcribe the wave energy energy-maximizing OCP into a finite-dimensional nonlinear program (NP).

Within moment-based theory, the external inputs affecting the WEC system (i.e., f_e and f_u) are expressed in terms of an implicit-form description. In particular, we define a signal generator $\mathscr{G}$ [sometimes referred to as an exogenous system (32)] described, for $t \in \mathbb{R}^+$, by the set of ν first-order equations

$$\mathscr{G} : \{\dot{\xi} = S\xi, \quad f_u = L_u\xi, \quad f_e = L_e\xi, \qquad 7.$$

with $\xi(t) \in \mathbb{R}^\nu$, $S \in \mathbb{R}^{\nu\times\nu}$, and $\{L_e^\intercal, L_u^\intercal\} \subset \mathbb{R}^\nu$. From now on, following Scarciotti & Astolfi (30), we adopt the following set of standing assumptions (SAs) for the signal generator in Equation 7: (*a*) the triple of matrices $(L_e - L_u, S, \xi(0))$ is minimal (SA1),[3] and (*b*) S is such that $\lambda(S) \subset \mathbb{C}^0$ with simple eigenvalues (SA2).

[3] Note that this implies the observability of $(S, L_e - L_u)$ and the excitability of $(S, \xi(0))$; for a formal treatment of excitability, we direct readers to Reference 33.

SA1 stems from the fact that the signal generator in Equation 7 does not have any input and is essentially driven by the initial condition $\xi(0)$. Given that this signal generator characterizes inputs to the WEC system under analysis, it is natural to construct Equation 7 in such a way that all the modes of motion described by the dynamic matrix S are excited and that the inputs generated are effectively observable. SA2 guarantees that the signal generator represented by Equation 7 produces bounded trajectories, which is also consistent with the practical nature of the WEC application: f_e is always bounded by virtue of the wave process itself, while f_u is ultimately user designed. Crucially, as discussed in Section 5, SA2 is also consistent with the oscillating nature of the harvesting process.

If SA1 and SA2 hold, and given that the zero equilibrium of the WEC system in Equation 6 is locally exponentially stable (see Remark 2), then there exists (10) a mapping π, locally[4] defined in a neighborhood Ξ of $\xi = 0$, with $\pi(0) = 0$, that is the solution of the (invariance) partial differential equation

$$\frac{\partial \pi(\xi)}{\partial \xi} S\xi = g(\pi(\xi), L_e\xi - L_u\xi) \qquad 8.$$

for all $\xi \in \Xi$, and the steady-state response of the interconnected WEC system represented by Equations 6 and 7 is $x_{ss}(t) = \pi(\xi(t))$ for any $x(0)$ and $\xi(0)$ sufficiently small. In particular, the mapping $\mathscr{Y} = C\pi$ is defined as the moment of the WEC system in Equation 6 at the signal generator $(S, L_e - L_u)$.

Remark 3. The moment $\mathscr{Y}$ of the WEC system in Equation 6 at the signal generator in Equation 7, computed along a particular trajectory $\xi(t)$, coincides with the (well-defined) steady-state response of the output of the WEC system, i.e., $y_{ss}(t) = \mathscr{Y}(\xi(t))$. This is exploited for control-oriented WEC modeling and optimal control synthesis in Sections 4 and 5, respectively.

In the special case in which the WEC system is described in terms of the linear dynamical operator in Equation 4, the invariance equation represented by Equation 8 essentially becomes a linear system of algebraic equations. In particular, the moment $\mathscr{Y}$ is such that $\mathscr{Y}(\xi) \equiv Y\xi$, with Y computed as

$$Y = (L_e - L_u)\Phi, \qquad 9.$$

where the matrix $\Phi \equiv \Phi(S, \mathcal{G})$ depends on both the specific parameters associated with the linear WEC equation shown in Equation 4 and the nature of the matrix S in Equation 7. For a detailed account of the computation of the matrix Φ, we direct readers to, e.g., Reference 29.

Remark 4. As in the nonlinear case (see Remark 3), the moment Y of the linear system in Equation 4 at the signal generator in Equation 7 is inherently linked to the steady-state output response of the WEC device, i.e., $y_{ss}(t) = Y\xi(t)$ for any particular trajectory $\xi(t)$.

4. MODEL REDUCTION FOR WAVE ENERGY CONVERTER SYSTEMS

Moments, as defined in Section 3.2, not only provide a specific parameterization of the steady-state output response for linear and nonlinear systems in terms of the state vector associated with the signal generator in Equation 7 but also play a crucial role in a state-of-the-art moment-matching-based model reduction framework. This set of model reduction techniques, based on the concept of a moment, involves the interpolation of the steady-state response of the output of the target

[4]All statements are local, although global versions can be straightforwardly derived.

system to be reduced, by leveraging the discussion in Remark 3. In particular, the reduced-order model obtained via moment matching has a steady-state response that matches the steady-state response of the system to be reduced, by sharing exactly the same moment for a given class of input signals.

4.1. Finite-Order Linear Parameterization

Recalling the discussion in Section 3.1 (particularly Remark 1), we note that the radiation impulse response function k_r, defining the WEC system $\mathcal{G}$ in Equation 4, is typically computed using BEM codes—i.e., only a finite number of data points characterizing k_r is available for modeling purposes. The presence of this nonparametric impulse term implies both a representative and a computational drawback for WEC control or estimation tasks, giving an overall input-to-state nonparametric representation.

To address this issue, and motivated by the linear time-invariant nature of the underlying radiation system, model reduction techniques can be employed, typically using a finite-dimensional state-space representation, which should ideally retain the underlying physical properties that characterize the WEC process. In particular, Faedo et al. (34) proposed a moment-matching-based solution for single-DOF devices, which was later extended to multi-DOF systems (35, 36) and WEC arrays (37). Furthermore, note that a critical comparison between this moment-based approach and a set of well-established techniques in the wave energy field (including, e.g., Reference 20) can be found in Reference 38.

To be precise, if the system is linear (as in the case discussed within this section), then the steady-state output response is fully characterized by the associated WEC frequency-domain response. In other words, as discussed in Section 3.2, since moments are in a one-to-one relation with the steady-state behavior of the target system, matching moments directly implies interpolation of the target frequency response at a finite number of points, here referred to as interpolation frequencies. Furthermore, as shown by Peña-Sanchez et al. (38) and Faedo et al. (39), essential physical properties of the device can be retained by (or enforced on) the reduced-order model by moment matching as a result of this frequency interpolation feature, such as internal stability, passivity, and zero dynamics—i.e., the approximating model is physically consistent.

In the following, we provide a brief account of the main elements involved in the computation of a reduced model by moment matching for the WEC system in Equation 4. In particular, following the set of standing assumptions for the corresponding signal generator $(S, L_e - L_u)$ outlined in Section 3.2, let both the inputs of $\mathcal{G}$ be defined in terms of Equation 7 with a matrix S such that $\lambda(S) = (j\mathscr{F}) \cup (-j\mathscr{F}) \subset \mathbb{C}^0$, where $\mathscr{F} = \{\omega_p\}_{p=1}^{f} \subset \mathbb{R}^+$ is a finite set of interpolation points, and hence $\#\mathscr{F} = 2f$. Leveraging the definition of a (linear) moment in Equation 9 and following Astolfi (10) and Scarciotti & Astolfi (30), we find that the family of reduced-order models

$$\tilde{\mathcal{G}} : \begin{cases} \dot{\Theta} = (S - \Delta L)\Theta + \Delta(f_e - f_u), \quad \theta = Y\Theta \approx y, \end{cases} \tag{10.}$$

where $L = L_e - L_u$ and Δ is any matrix such that $\lambda(S) \cap \lambda(S - \Delta L) = \emptyset$, contains all the models of dimension ν interpolating the moments of the WEC system at (S, L).

Remark 5. The family of models in Equation 10 is conveniently parameterized in terms of the matrix Δ, which can be used to enforce specific properties in the reduced-order model, such as matching with a prescribed set of eigenvalues Λ, i.e., to guarantee that $\lambda(S - \Delta L) = \Lambda$. The specific choice of Δ for the WEC application case can be performed in terms of an offline optimization procedure (as discussed in, e.g., Reference 34). Furthermore, Faedo et al. (39) included a specific algorithm for enforcing passivity and zero dynamics, incorporating all the relevant WEC physical properties into the computed moment-based parametric structure.

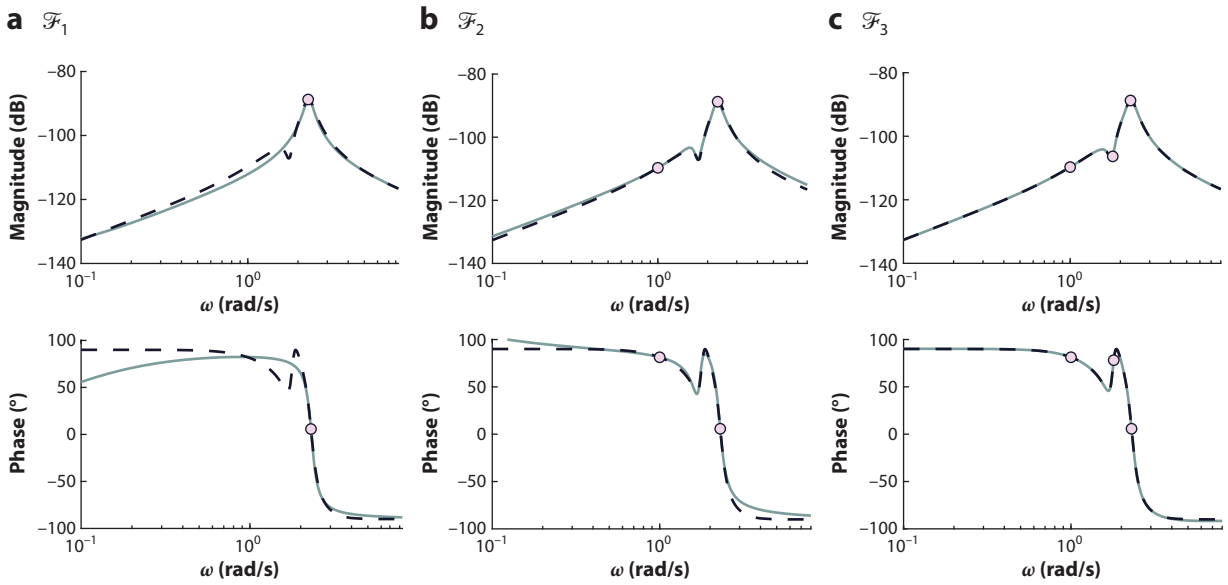

Figure 3

Parameterization by moment matching for the Ocean Power Technologies WEC case with different sets of interpolation points for (*a*) $\mathscr{F}_1$, (*b*) $\mathscr{F}_2$, and (*c*) $\mathscr{F}_3$. Abbreviation: WEC, wave energy converter. Figure adapted from Reference 41.

Remark 6. The reduced-order model in Equation 10 has dimension $\nu = 2f = \#\mathscr{F}$, where f is the number of (user-selected) interpolation points in $\mathscr{F}$. This is a consequence of the fact that, for each frequency ω_i, both positive and negative $j\omega_i$ are chosen as eigenvalues of the real-valued matrix S.

To briefly illustrate the moment-based finite-order parameterization method described above, we present a case study based on a toroidal WEC geometry, which constitutes one of the main components of a large class of devices, including, for instance, the well-known Ocean Power Technologies point absorber WEC (40). The choice of the set of interpolation points (frequencies) can be made by analyzing the gain of the target frequency response and selecting points that characterize dynamically important features of the underlying WEC. A sensible selection includes, for instance, the resonant frequency of the device under consideration. Note that this is, effectively, the frequency where the maximum amplification occurs, i.e., the frequency characterizing the $\mathscr{H}_\infty$-norm of the WEC system $\mathcal{G}$. Based on the provided discussion, different sets of interpolation frequencies within this example case are chosen as follows: $\mathscr{F}_1 = \{2.3\}$, $\mathscr{F}_2 = \{1, 2.3\}$, and $\mathscr{F}_3 = \{1, 1.8, 2.3\}$, with the property that $\mathscr{F}_1 \subset \mathscr{F}_2 \subset \mathscr{F}_3$. As can be appreciated from **Figure 3**, the set $\mathscr{F}_1$ already includes a key interpolation point, i.e., the resonant frequency associated with the DOF under analysis. $\mathscr{F}_2$ includes an additional low-frequency component, while the set $\mathscr{F}_3$ further expands $\mathscr{F}_2$ by including a midfrequency component. As expected from the theoretical foundations of this moment-based strategy, the approximating models have exactly the same frequency-domain behavior as the target model for each element of the corresponding interpolation set $\mathscr{F}$, with a clear decrease in the overall approximation error from $\mathscr{F}_1$ to $\mathscr{F}_3$.

4.2. Nonlinear Model Reduction

If, instead of considering the linear operator in Equation 4, we assume that the WEC system is described in terms of the general nonlinear system in Equation 4 (or, equivalently, Equation 6), then the chosen representation not only is nonparametric (as discussed in Section 4.1) but also

can present complex nonlinear effects arising from a diversity of modeling considerations (see Section 3.1). Ultimately, depending on the nature of these terms, the specific WEC representation can preclude both a well-posed control or estimation synthesis and the consequent real-time implementation—i.e., there is a limit to the analytical complexity for which a controller or estimator can be effectively synthesized and handled in real time.

The nonlinear moment-based framework, recalled in Section 3.2, has been recently shown to be a valuable tool for model reduction of nonlinear WECs, with a pioneering application (42), given the inherent preservation of steady-state response characteristics. In particular, by exploiting the corresponding definition of a (nonlinear) moment analogously to Equation 10 [leveraging the same choice of $\lambda(S)$], and following Astolfi (10) and Scarciotti & Astolfi (30), we can define a family of reduced models for the nonlinear WEC system in Equation 6 that achieve moment matching at (S, L) as

$$\tilde{\mathcal{G}} : \begin{cases} \dot{\Theta} = (S - \Delta L)\Theta + \Delta(f_{\mathrm{e}} - f_{\mathrm{u}}), \\ \theta = \mathscr{Y}(\Theta) \approx y. \end{cases} \tag{11.}$$

Note that the family of models in Equation 11, also parameterized in terms of a constant matrix Δ (per Equation 10), is described by a linear differential equation with a nonlinear output map, i.e., a Wiener model. Furthermore, given the linear nature of Δ, the determination of $\tilde{\mathcal{G}}$ essentially reduces to the computation of the mapping $\mathscr{Y}$.

Clearly, the availability of $\mathscr{Y}$ in Equation 11 implies the availability of a closed-form solution of the associated partial differential equation shown in Equation 8, which is far from trivial for the rather generic nonlinear WEC model in Equation 6. To address this issue, Faedo et al. (42) proposed a Galerkin procedure for the computation of an approximation of $\mathscr{Y}$, based on the approximation framework for nonlinear moments presented in Reference 43. To briefly summarize, it is assumed that the moment of the WEC system can be reasonably described in terms of a finite-dimensional function space $\mathscr{H}$ (equipped with an inner-product operation), generated by a family of $N_{\mathcal{I}}$ continuous basis functions $\{\xi \mapsto \phi_i(\xi)\}_{i \in \mathcal{I} \subset \mathbb{N}}$, $\#\mathcal{I} = N_{\mathcal{I}}$, i.e.,

$$\mathscr{Y}(\xi) \approx \widetilde{\mathscr{Y}}(\xi) = \sum_{i \in \mathcal{I}} \alpha_i \phi_i(\xi). \tag{12.}$$

The set of coefficients $\{\alpha_i\}_{i \in \mathcal{I}} \subset \mathbb{R}$, corresponding with the ansatz shown in Equation 12, is computed by following a Galerkin procedure, i.e., by projecting a well-defined residual equation (constructed in terms of the partial differential equation shown in Equation 8) over $\mathscr{H}$. Faedo et al. (42) defined the set of functions $\{\phi_i\}$ in terms of polynomial functions of the state vector of the associated signal generator in Equation 7 with a user-defined maximum degree, hence providing full control of the underlying characteristics of the reduced structure.

Adopting a similar set of assumptions, Faedo et al. (44) and Papini et al. (45) proposed a data-driven model reduction by moment matching for WEC systems based on the theoretical framework of Scarciotti et al. (46). In particular, the same family of models represented by Equation 11 was considered, including the approximation of $\mathscr{Y}$ in terms of a finite-dimensional function space (i.e., Equation 12). The main difference resides in the fact that the associated set of coefficients $\{\alpha_i\}$ is computed by exploiting measurements of the steady-state response of the WEC system, in contrast to the analytic Galerkin formulation of Faedo et al. (42, 43). This allows for an approximation of the nonlinear WEC model $\mathcal{G}$ even in the case where the associated state transition map f is only partially known (or even completely unknown) and is a powerful tool for data-driven WEC modeling.

We briefly exemplify the moment-based nonlinear reduction procedure described above by means of the (data-driven) case study analyzed by Papini et al. (45), based on a CorPower-like wave energy absorption system (23) schematically illustrated in **Figure 4** along with a

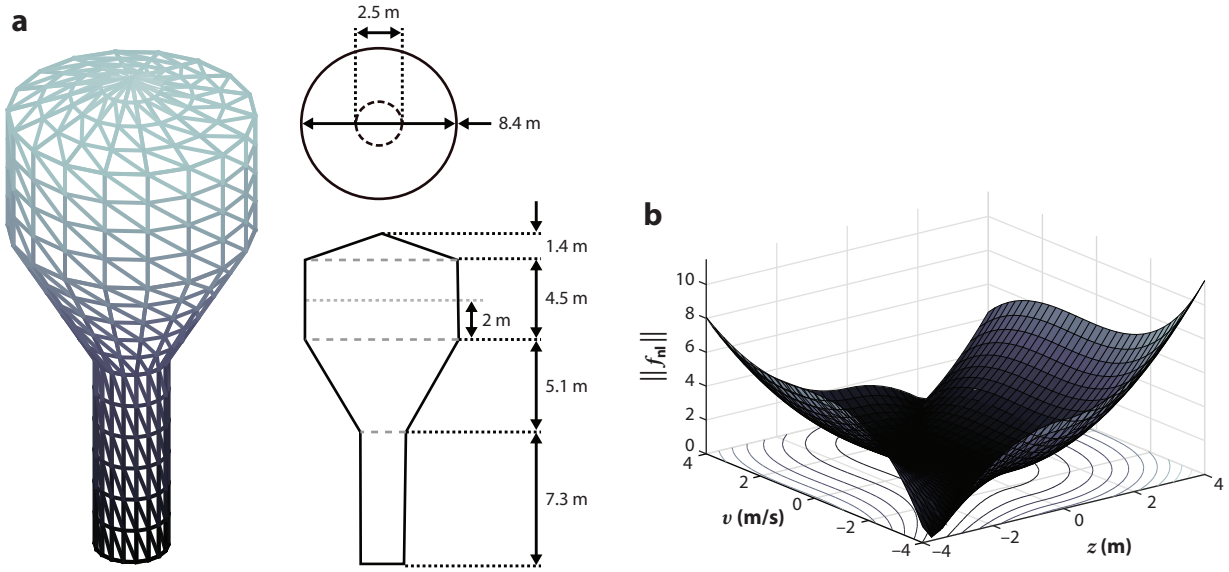

Figure 4

(*a*) Schematic illustration of the CorPower-like device considered in the nonlinear model reduction case study. (*b*) Graphical appraisal of the nonlinear map f_{nl} considered in the case study, which is composed of both viscous effects and nonlinear restoring forces (see Section 3.1). Figure adapted from Reference 45 (CC BY 4.0).

graphical appraisal of the nonlinear map f_{nl} considered. We assume that the signal generator in Equation 7 is described in terms of a single frequency component ω_w characterizing the behavior of the system under a monochromatic wave field, i.e., $\lambda(S) = \{\pm j\omega_w\}$, and hence $\xi(t) \in \mathbb{R}^2$. Several initial conditions for the resulting signal generator (Equation 7) are considered, in order to explore the operational space of the WEC system, according to the defined sea-state conditions. For each of these scenarios, the corresponding steady-state outputs are collected and used in a least-squares procedure for computation of the approximating moment $\tilde{\mathscr{Y}}$, described as in Equation 12.

In particular, polynomials in (ξ_1, ξ_2) are considered for the definition of the associated function space $\mathscr{H}$. **Figure 5*a*** shows the corresponding approximation for the moment in terms of a smooth manifold, and **Figure 5*b*** shows output time traces for a particular wave input realization along with the evolution of the absolute value of the approximation error. It can be appreciated that, once the transient period extinguishes, the target and approximating time traces become almost indistinguishable, as would be expected from the described moment-matching-based model reduction procedure.

5. CONTROL FOR WAVE ENERGY CONVERTER SYSTEMS

As discussed in Section 1, the overall control objective for WEC systems is typically written in terms of maximization of mechanical energy absorption, in turn minimizing the associated WEC levelized cost of energy (see, e.g., 4, 47). To be precise, the WEC control problem can be generally written, for a given time interval $\Omega = [0,\ T_0] \subset \mathbb{R}^+$, in terms of the following OCP:

$$\begin{aligned} \{y^{\mathrm{opt}}, f_{\mathrm{u}}^{\mathrm{opt}}\} &= \arg\max_{\{y, f_{\mathrm{u}}\}} E(y, f_{\mathrm{u}}), \\ \text{subject to:} \quad &\text{WEC dynamics } \mathcal{G} : \{\dot{x} = f(x, f_{\mathrm{e}} - f_{\mathrm{u}}), \quad y = Cx, \\ &\text{Constraints } \mathscr{S} : \{(y, f_{\mathrm{u}}) \in \mathscr{X} \times \mathscr{F}_{\mathrm{u}}, \quad \forall t \in \Omega, \end{aligned} \tag{13.}$$

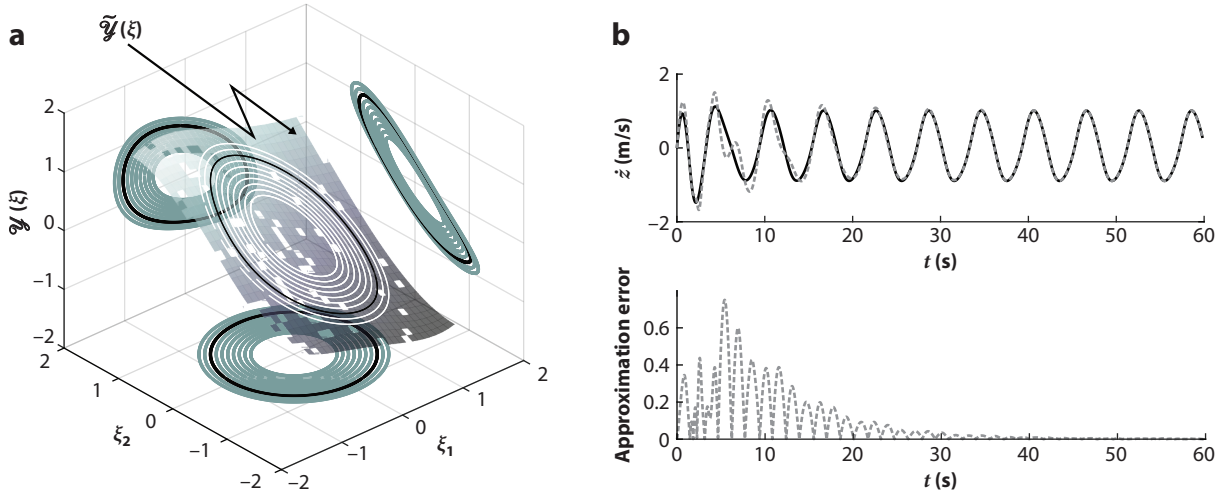

Figure 5

Performance of the data-driven nonlinear model reduction by moment matching for WECs. (*a*) The approximation for the moment in terms of a smooth manifold. (*b*, *top*) Output time traces for both the target nonlinear (*solid black line*) point absorber system $\mathcal{G}$ and the moment-based reduced-order model (*dashed gray line*) in Equation 11 with the corresponding approximating moment $\tilde{\mathcal{Y}}$ for a particular wave input realization. (*b*, *bottom*) The evolution of the absolute value of the approximation error. Abbreviation: WEC, wave energy converter. Figure adapted from Reference 45 (CC BY 4.0).

where we recall that $y = \dot{z}$ (i.e., the device velocity), and the map E represents the average mechanical energy of the WEC system, i.e.,

$$E(y, f_u) = \frac{1}{T_0}\int_\Omega y(\tau) f_u(\tau) d\tau. \qquad 14.$$

The notation y^{opt} and f_u^{opt} is used to represent the optimal velocity of the WEC system and the optimal velocity under the optimal energy-maximizing control solution, respectively. The sets $\mathcal{X}$ and $\mathcal{F}_u$ represent the admissible values for output and input variables (i.e., constraints), respectively, that are included in the OCP to guarantee the safe operation of the WEC device and associated PTO system.

Clearly, the OCP in Equation 13 is defined over an infinite-dimensional space. The underlying idea, first posed for linear WEC systems by Faedo et al. (29), is to use the parameterization of the steady-state response of the WEC system in terms of moments to provide a transcription of Equation 13 into a finite-dimensional NP carried over the function space induced by the signal generator in Equation 7. The objective of this section is to provide an overview of how moment-based theory for WECs, as presented in Section 3.2, can be effectively used to compute an approximate solution of Equation 13 for a wide variety of WEC models and operating conditions, as detailed in the following.

5.1. Linear Wave Energy Converter Control

As briefly introduced in Section 5, the main idea, originally posed by Faedo et al. (29), is to solve the problem shown in Equation 13 by exploiting the steady-state parameterization of the WEC system in terms of the corresponding moment. To be precise, we replace the dynamical behavior of the WEC system $\mathcal{G}$ with the associated moment-based equation (i.e., either Equation 8 or Equation 9, depending on the nature of $\mathcal{G}$). To achieve this, the first step is to define a signal generator (Equation 7) to provide an implicit-form description for the wave excitation force input

f_e and, consequently, the applied control input f_u. Motivated by the harmonic nature of the wave process (see, e.g., 15, 48), the matrix of the associated signal generator is described in terms of a finite number of harmonics of a given fundamental frequency $\omega_0 = 2\pi/T_0 \in \mathbb{R}$, i.e.,

$$S = \bigoplus_{p=1}^{f} \begin{bmatrix} 0 & p\omega_0 \\ -p\omega_0 & 0 \end{bmatrix}, \tag{15.}$$

so that $\lambda(S) = \{\pm jp\omega_0\}$, in line with SA2 (see Section 3.2).

Remark 7. One can verify that, under SA1, the dynamic matrix shown in Equation 15 is such that

$$\mathcal{X} = \text{span}\big(\{\xi_i(t)\}_{i\in\mathbb{N}_v}\big) = \text{span}\big(\{\cos(p\omega_0 t), \sin(p\omega_0 t)\}_{p\in\mathbb{N}_f}\big) \tag{16.}$$

so that f_e and f_u are essentially described in terms of a T_0-periodic map in Ω.

Formally, for the case of the linear WEC model in Equation 4 with the signal generator in Equation 7, matrix S in Equation 15, and associated moment computation in Equation 9, the OCP in Equation 13 can be transcribed to the following steady-state formulation:

$$\begin{aligned} \{Y^{\text{opt}}, L_u^{\text{opt}}\} &= \arg\max_{\{Y,L_u\}} E(Y\xi, L_u\xi), \\ \text{subject to:} \quad &\text{Moment-based equation} : Y = (L_e - L_u)\Phi, \\ &\text{Constraints} : \big\{(Y\xi, L_u\xi) \in \mathcal{X} \times \mathcal{F}_u, \quad \forall t \in \Omega, \end{aligned} \tag{17.}$$

where the corresponding optimal output and input maps can be computed as $y^{\text{opt}} = Y^{\text{opt}}\xi$ and $f_u^{\text{opt}} = L_u^{\text{opt}}\xi$. We further note that, due to the nature of the space of functions generated by the entries of the state vector associated with the signal generator with the matrix in Equation 15 (see Remark 7), the relation (29)

$$E(y, f_u) \mapsto E(Y\xi, L_u\xi) = \frac{1}{T_0}\int_\Omega Y\xi(\tau)L_u\xi(\tau)\mathrm{d}\tau = \frac{1}{2}Y^{\mathrm{T}}L_u, \tag{18.}$$

holds. Leveraging the result recalled in Equation 18, we can further write the transcribed OCP in Equation 17 in terms of the finite-dimensional NP:

$$\begin{aligned} \{Y^{\text{opt}}, L_u^{\text{opt}}\} &= \arg\max_{\{Y,L_u\}} \frac{1}{2}Y^{\mathrm{T}}L_u, \\ \text{subject to:} \quad &\text{Moment-based equation} : Y = (L_e - L_u)\Phi, \\ &\text{Constraints} : \big\{(Y\xi, L_u\xi) \in \mathcal{X} \times \mathcal{F}_u, \quad \forall t \in \widetilde{\Omega} \subset \Omega, \end{aligned} \tag{19.}$$

where $\widetilde{\Omega} = \{t_i\}_{i\in\mathcal{I}_\Omega}$, $\#\mathcal{I}_\Omega = N_c$, represents a finite set of collocation instants used to enforce the constraints in Equation 13, now parameterized in terms of the corresponding signal generator. If the moment-based equation in Equation 19 is effectively included directly as part of the corresponding mapped objective, it is possible to show that the transcribed NP is of a quadratic type, i.e., can be written in terms of a quadratic program (QP) in L_u. Furthermore, such a QP is inherently concave due to the nature of the WEC conversion process (i.e., the passivity property of $\mathcal{G}$; see the discussion in Section 4.1 and Reference 29).

Remark 8. The underlying concave QP nature of Equation 19 is a fundamental feature of this moment-based transcription process. In particular, due to the nature of the chosen signal generator and the connection between moments and steady-state response, the transcribed problem effectively has a unique globally optimal solution, allowing for the utilization of efficient numerical optimization routines (see, e.g., 49) to compute a solution to the energy-maximizing WEC control problem. Note that

this is typically not the case in other direct optimal control techniques, where regularization terms are used to guarantee the existence of a unique solution (see the discussion in Section 1).

5.2. Nonlinear Wave Energy Converter Control

If, instead of considering the linear operator in Equation 4, we assume that the WEC system is described in terms of the general state-space description (Equation 6), the procedure outlined in Section 5.1 can be followed analogously, with some fundamental differences, as outlined in the remainder of this section. In particular, in accordance with the linear case in Section 5.1, the idea is to replace the dynamical constraint in Equation 13 with the corresponding moment, which can now be computed in terms of the nonlinear partial differential equation shown in Equation 8, as opposed to the linear equation shown in Equation 9. The reader can appreciate that there is an immediate difficulty in following these steps: This pathway would require a closed-form expression for the moment $\mathscr{Y}$, which is, as discussed for the nonlinear model reduction case in Section 4.2, generally impossible to compute. Faedo et al. (50) explicitly solved this problem for the WEC control case by leveraging the approximation technique proposed in Reference 43. We briefly discuss the main underlying elements in Reference 50, in particular the definition of the so-called extended signal generator $\overline{\mathscr{G}}$, as follows:

$$\overline{\mathscr{G}}: \begin{cases} \dot{\overline{\xi}} = \overline{S}\overline{\xi}, \quad f_{\mathrm{e}} = \overline{L_{\mathrm{e}}}\overline{\xi}, \quad f_{\mathrm{u}} = \overline{L_{\mathrm{u}}}\overline{\xi}, \\ \overline{S} = S \oplus \left(\bigoplus_{p=f+1}^{\overline{f}} \begin{bmatrix} 0 & p\omega_0 \\ -p\omega_0 & 0 \end{bmatrix} \right), \\ \overline{L_{\mathrm{e}}} = \begin{bmatrix} L_{\mathrm{e}} & 0 \end{bmatrix}, \quad \overline{\xi}(0) = \begin{bmatrix} \xi(0)^{\mathsf{T}} & \overline{\xi}_0^{\mathsf{T}} \end{bmatrix}^{\mathsf{T}}, \end{cases} \tag{20.}$$

where the pair of matrices $(\overline{S}, \overline{\xi}(0)) \in \mathbb{R}^{\overline{\nu}\times\overline{\nu}} \times \mathbb{R}^{\overline{\nu}}$ is excitable.

The system in Equation 20 is an extension of the signal generator in Equation 7 (with the matrix in Equation 15) in the following sense: Consider the definition of the induced space $\mathcal{X}$ in Equation 16, and let $\overline{\mathcal{X}} = \mathrm{span}\{\overline{\xi}_i\}_{i\in\mathbb{N}_{\overline{\nu}}}$. It is straightforward to see that $\lambda(S) \subset \lambda(\overline{S})$ and, given the excitability condition on the pairs $(S, \xi(0))$ and $(\overline{S}, \overline{\xi}(0))$, that $\mathcal{X} \subset \overline{\mathcal{X}}$. Furthermore,

$$\overline{\mathcal{X}} = \mathcal{X} \cup \mathrm{span}\big(\{\cos(p\omega_0 t), \sin(p\omega_0 t)\}_{p=f+1}^{\overline{f}}\big), \tag{21.}$$

so that the signal generator $\overline{\mathscr{G}}$ extends $\mathscr{G}$ by including a larger set of harmonics of the fundamental frequency ω_0 in the state space associated with such an implicit-form description.

Remark 9. Note that f_{e}, originally written in terms of the signal generator in Equation 7, with matrix S in Equation 15, is defined in terms of the extended structure $\overline{\mathscr{G}}$ by simply leveraging a suitable inclusion operator $L_{\mathrm{e}} \mapsto \overline{L_{\mathrm{e}}}$.

Using the extended generator in Equation 20, we can write an associated moment equation (as in Equation 8) for the definition of the corresponding moment. Furthermore, for a given trajectory $\overline{\xi}(t)$, Faedo et al. (50) proposed the following approximation:

$$y_{\mathrm{ss}}(t) = \mathscr{Y}(\xi(t)) \approx \overline{Y}\overline{\xi}(t), \tag{22.}$$

where the approximated moment $\overline{Y}$ is computed in terms of a nonlinear algebraic system of equations of the form

$$\mathcal{R}(\overline{Y}, \overline{L_{\mathrm{u}}}) = 0. \tag{23.}$$

The residual map $\mathcal{R}$ in Equation 23 is defined in terms of the nonlinear dynamics of the WEC system in Equation 6 (or, alternatively, Equation 5) and projected onto the space induced by $\overline{\mathscr{X}}$ in Equation 21, giving origin to Equation 23, i.e., in a Galerkin-like procedure. As demonstrated by Faedo et al. (50), uniform convergence toward $y_{ss}(t)$ can be guaranteed for a given trajectory $\overline{\xi}(t)$ as $\overline{\nu} \to \infty$ in Equation 20, i.e., by modifying the dimension (order) of the associated extended generator.

Considering the approximation in Equations 22 and 23, we can then transcribe the OCP in Equation 13 into a finite-dimensional NP by leveraging the connection between moments and steady-state behavior, i.e.,

$$\begin{aligned} \{\overline{Y}^{\text{opt}}, \overline{L_{\text{u}}}^{\text{opt}}\} &= \arg\max_{\{\overline{Y}, \overline{L_{\text{u}}}\}} \frac{1}{2}\overline{Y}^{\text{T}}\overline{L_{\text{u}}}, \\ \text{subject to:} \quad & \text{Moment-based equation} : \mathcal{R}(\overline{Y}, \overline{L_{\text{u}}}) = 0, \\ & \text{Constraints} : \left\{(\overline{Y\xi}, \overline{L_{\text{u}}\xi}) \in \mathscr{X} \times \mathscr{F}_{\text{u}}, \quad \forall t \in \widetilde{\Omega} \subset \Omega. \right. \end{aligned} \tag{24.}$$

Remark 10. Using standard assumptions with respect to the nonlinear map f_{nl} and characterizing the WEC model in Equation 5, one can show that the transcribed OCP in Equation 24 can be written in terms of a concave QP program plus a nonlinear bounded term. Using this decomposition, Faedo et al. (50) showed that Equation 24 always admits an energy-maximizing solution, also giving explicit conditions for global optimality. This allows for the application of efficient numerical routines for the computation of the moment-based solution (e.g., 51).

Application of this nonlinear framework, apart from the pioneering Reference 50, can also be found in References 52 and 53, which additionally include relevant extensions to the original class of nonlinear effects considered in Reference 50. In particular, Reference 52 includes nonlinear PTO effects in terms of an efficiency map characterizing the mechanical-to-electrical energy conversion, exploiting the physical arguments in Reference 54. On the other hand, Reference 53 effectively includes nonlinear Froude–Krylov effects (both static and dynamic; see Reference 22) by leveraging a data-based modeling approach suited for the moment-based transcription method.

5.3. Real-Time Implementation: The Receding-Horizon Formulation

As discussed in Section 3.1, the wave excitation force f_{e} is virtually always unmeasurable, requiring both estimation and forecasting to compute instantaneous and future values within a given set Ω, respectively, for effective computation of the associated optimal control input. Within the presented moment-based framework, this implies knowledge of the associated implicit-form description for f_{e}, in terms of the signal generator in Equation 7. In particular, to solve the OCP in real time, accommodating a corresponding estimate of f_{e}, Faedo et al. (55) proposed a receding-horizon formulation of the moment-based transcription described in Sections 5.1 and 5.2. This was later exploited by Mosquera et al. (56) and Faedo et al. (57), who generated the optimal laws $\{y^{\text{opt}}, f_{\text{u}}^{\text{opt}}\}$ within a sliding window and fed them as optimal references to a lower tracking loop. In particular, both works considered higher-order sliding-mode controllers to achieve robust reference tracking in finite time.

To be precise, Faedo et al. (55) wrote the set Ω in Equations 19 and 24 as $\Omega_K = [K\Delta_{\text{h}}, K\Delta_{\text{h}} + T_0] \subset \mathbb{R}^+, K \in \mathbb{N}$, where T_0 denotes, in this case, the length of the Kth time window (i.e., the time horizon) in which Equation 13 is effectively maximized, and where Δ_{h} denotes the receding time step. The receding-horizon reference generation procedure is then as follows:

1. Solve Equations 19 and 24 for the time window Ω_K—i.e., compute the set $\mathscr{R}_K : \{y^{\text{opt}}, f_{\text{u}}^{\text{opt}}\}$.
2. Provide the reference set $\mathscr{R}_K$ for the inner tracking loop in the interval $[K\Delta_{\text{h}}, (K+1)\Delta_{\text{h}}] \subset \mathbb{R}^+$, i.e., for a single receding-horizon step Δ_{h}.
3. Move $\Omega_K \mapsto \Omega_{K+1}$ and go back to step 1.

While the T_0-periodicity nature for f_{e}, arising from the (harmonic) implicit-form representation in Equation 20, has been shown to be valid for sufficiently large T_0 in numerous studies (see, e.g., 48, 58), within the receding-horizon OCP formulations associated with Equations 19 and 24, the length of the time window is commonly chosen following a rather conservative approach, to keep the associated computational requirements within real-time limits. This, in turn, naturally creates an issue when attempting to represent f_{e} in terms of the implicit form of Equation 20. Faedo et al. (55) addressed this issue by exploiting windowing functions: Suppose we analyze f_{e} within a single window (time interval) Ω_K. Within this set, we define the so-called apodized (i.e., windowed) wave excitation force f_{e}^{ϑ} as

$$f_{\text{u}}^{\vartheta} = f_{\text{u}}\vartheta, \ \forall t \in \Omega_K, \tag{25.}$$

where the map $\vartheta : \Omega_K \to [0, 1]$ is used to smoothly bring f_{e} down to zero at the edges of the set Ω_K, so that the derivative of its corresponding T_0-periodic extension is sufficiently smooth (59). Finally, following Faedo et al. (55), we can bring f_{e}^{ϑ} (approximately) to the implicit form of Equation 20 by orthogonal projection on the set spanned by $\overline{\mathcal{X}}$, to subsequently solve Equations 19 and 24 accordingly, for each Ω_K.

5.4. Robustifying the Control Solution

WEC models, as derived based on Section 3.1, are inherently affected by uncertainty, particularly arising in the hydrodynamic modeling stage. This is due to the relatively restrictive set of assumptions MA1–3, used to arrive at the simplified representation given by Cummins (see Section 3.1). Furthermore, system uncertainty is not the sole source of uncertainty intrinsically affecting the WEC control problem. In particular, given that f_{e} is virtually always unmeasurable, estimates are sought via estimation and forecasting techniques (see the discussion in Section 5.3), so that uncertainty in the information fed to the corresponding OCP is also ubiquitous. Sections 5.4.1 and 5.4.2 now discuss the system and input uncertainty cases, respectively, offering an overview of the set of robust moment-based solutions available for WECs.

5.4.1. System uncertainty. We begin by assuming that the linear WEC equation $\mathcal{G} \equiv \mathcal{G}^0$ (Equation 4) can be adopted as a nominal model of the device, with a corresponding (nominal) linear moment equation given in terms of Equation 9 (i.e., $Y \equiv Y^0$), associated with a nominal output $y \equiv y^0$. In a more realistic scenario, the model describing the WEC dynamics is affected by modeling errors, which can be written in terms of a suitably defined uncertainty. In particular, we consider that the nominal WEC system is perturbed by a multiplicative output uncertainty map (41, 60), characterized in terms of a stable linear time-invariant system H^{δ}, with input y^0 and output d^{Δ}, and corresponding moment at Equation 7 given by $D^{\delta} = Y^0\delta$. This is schematically illustrated in **Figure 6**.

Within this formulation, and analogous to Equation 9, the moment Y^{δ} of the uncertain WEC system is essentially written as

$$Y^{\delta} = Y^0 + Y^0\delta = (L_{\text{e}} - L_{\text{u}})\Phi(\mathbb{I} + \delta). \tag{26.}$$

The uncertainty, defined via the stable system H^{δ}, is then fully parameterized in terms of δ and directly affects the moment-based representation of the nominal WEC system in Equation 4. If we further assume $\delta \in \mathcal{P}$, with $\mathcal{P}$ a convex polytope defined as the convex hull of a finite set

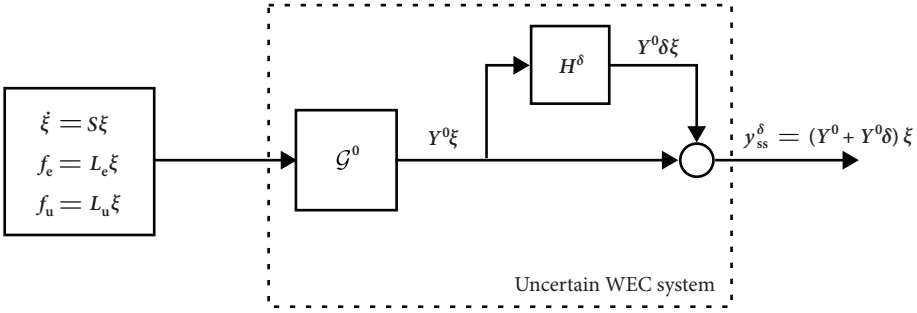

Figure 6

Schematic representation of the uncertain WEC system. Abbreviation: WEC, wave energy converter. Figure adapted from Reference 41.

of N_V vertices, i.e., $\mathcal{P} = \text{conv}(V_\mathcal{P})$, $\#V_\mathcal{P} = N_V$, then the moment-based robust formulation of the problem in Equation 19 can be written following a worst-case performance (WCP) approach (61). The underpinning concept behind this approach, which originated in the field of decision theory and is known as Wald's minimax (or maximin) paradigm (62), essentially optimizes a given objective for the worst-case scenario with respect to the defined uncertainty. In the spirit of the WCP method, the robust moment-based energy-maximizing formulation for uncertain WEC systems can be defined in terms of Equation 26 as follows:

$$\begin{aligned} \{Y^{\delta\text{opt}}, L_u^{\delta\text{opt}}\} = \arg\max_{\{Y^\delta, L_u\}} \arg\min_{\delta\in V_\mathcal{P}} \frac{1}{2} Y^{\delta\text{T}} L_u, \\ \text{subject to:} \quad \text{Uncertain moment-based equation} : Y^\delta = (L_e - L_u)\Phi(\mathbb{I} + \delta), \\ \text{Constraints} : \left\{(Y^\delta\xi, L_u\xi) \in \mathcal{X} \times \mathcal{F}_u, \quad \forall(\delta, t) \in V_\mathcal{P} \times \widetilde{\Omega}, \right. \end{aligned} \tag{27.}$$

where the NP in Equation 27 computes the worst-case scenario for the WEC energy-maximizing problem with respect to every possible uncertainty δ in the polytope $\mathcal{P}$.

With mild assumptions on the nature of the uncertainty δ, it is possible to show that Equation 27 can be written as a max-min problem composed of a concave QP problem in L_u and a linear program (LP) in δ. This has a very important implication, which is already reflected in the transcription in Equation 27: The unique solution of the robust moment-based WEC formulation is reached precisely on the convex hull of the uncertainty set $\mathcal{P}$—i.e., the solution lies precisely at one of the vertices $V_\mathcal{P}$. This essentially means that it is sufficient to solve the NP in Equation 27 only for the N_V elements of the finite set $V_\mathcal{P}$.

We exemplify the robust moment-based solution in the following, based on Reference 63. Consider a spherical heaving point absorber under regular wave excitation, represented in terms of the implicit form of Equation 7, with matrix S as in Equation 15 and a single frequency component ω_0. Let s_h^0 denote the nominal hydrostatic stiffness of such a system, and suppose its actual value is such that $s_h \in \mathcal{S}_h$, with $\mathcal{S}_h = [-1.3s_h^0, 1.3s_h^0] \subset \mathbb{R}$—i.e., it can vary within $\pm 30\%$ of its nominal value s_h^0. **Figure 7*a*** illustrates the polytope $\mathcal{P} \subset \mathbb{R}^2$ for the defined hydrostatic stiffness uncertainty, plotted in terms of its set of vertices, along with the nominal value for the hydrostatic stiffness; **Figure 7*b*** illustrates the results of nominal and robust moment-based control performance in terms of energy absorption, considering various levels of uncertainty for the parameter s_h, represented as a percentage deviation from its nominal value s_h^0. The WCP, for all cases, occurs when the parameter s_h deviates by -30% from its nominal value. Note that the optimal WCP is achieved by

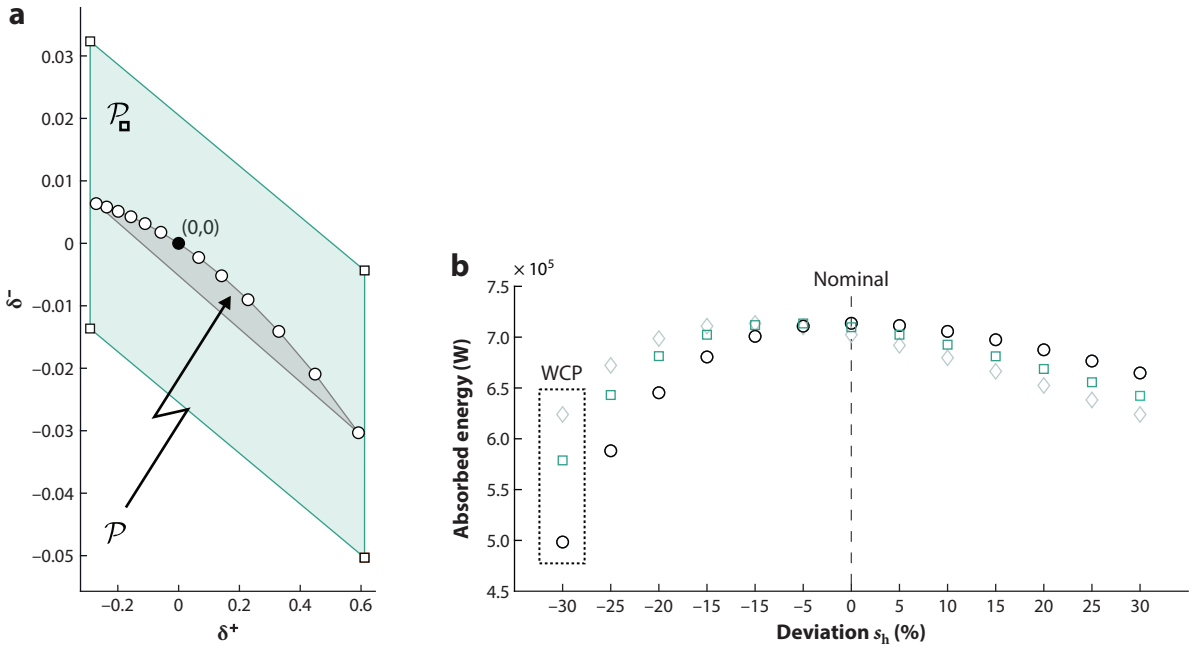

Figure 7

(*a*) The uncertainty polytope $\mathcal{P} \subset \mathbb{R}^2$ for the defined hydrostatic stiffness uncertainty (*gray shading*), plotted in terms of its set of vertices (*open circles*). The nominal value for the hydrostatic stiffness is represented by the point in $\mathbb{R}^2$ corresponding with zero uncertainty (*filled circle*). (*b*) The results of nominal and robust moment-based control performance in terms of energy absorption, considering various levels of uncertainty for the parameter s_h, represented as a percentage deviation from its nominal value s_h^0. The nominal performance is indicated by black circles. Two distinct robust performance cases are presented: one based on computing a moment-based control solution considering the polytope $\mathcal{P}$ (*gray diamonds*) and a more conservative case, represented by the polytope $\mathcal{P}_\square$, as shown in panel *a* (*green squares*). Abbreviation: WCP, worst-case performance. Figure adapted from Reference 41.

employing the robust energy-maximizing strategy computed with the polytope $\mathcal{P}$, based on prior knowledge of the range of variation of the uncertain parameter, while a clear drop in performance (in terms of WCP) can be directly observed for the case where the more conservative polytope $\mathcal{P}_\square$ is considered.

5.4.2. Input uncertainty. For the case of input uncertainty, one can pursue an analogous formulation to that presented in Section 5.4.1 for the case of system uncertainty. In particular, it is assumed that the WEC system is driven by what is now referred to as the nominal signal generator $\mathcal{G} \equiv \mathcal{G}^0$ in Equation 7, which is associated with a nominal wave excitation force input $f_e = f_e^0$. Similarly to Section 5.4.1, a multiplicative output uncertainty framework is considered (see 41, 63), as illustrated schematically in **Figure 8**.

Within this formulation, the output vector describing the uncertain wave excitation force $f_e^\delta = L_e^\delta \xi$ is essentially written as $L_e^\delta = L_e^0 + L_e^0 \delta$, so that the corresponding moment for the overall uncertain WEC system can be computed in terms of the following relation:

$$Y^\delta = (L_e^0 + L_e^0 \delta)\Phi. \qquad 28.$$

Following a WCP approach, as for the case of system uncertainty in Section 5.4.1, we can write the robust moment-based formulation for the case of input uncertainty in terms of the following

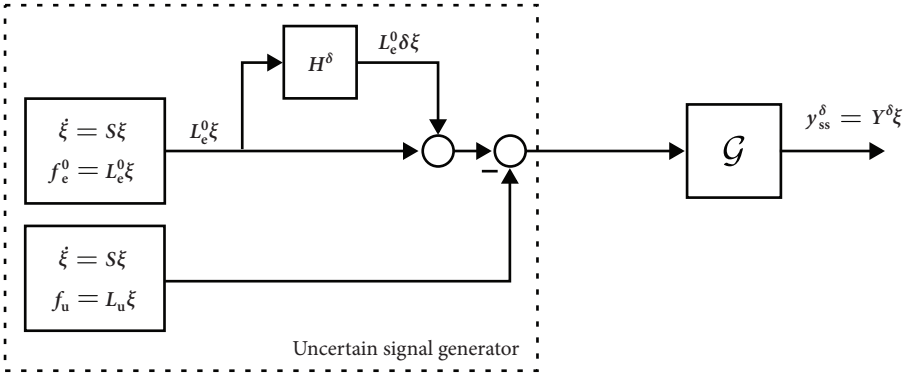

Figure 8

Schematic representation of the uncertain signal generator. Figure adapted from Reference 41.

min-max problem:

$$\{Y^{\delta\text{opt}}, L_u^{\delta\text{opt}}\} = \arg\max_{\{Y^\delta, L_u\}} \arg\min_{\delta\in V_\mathcal{P}} \frac{1}{2} Y^{\delta\mathrm{T}} L_u,$$

$$\text{subject to:} \quad \text{Uncertain moment-based equation} : Y^\delta = (L_e^0 + L_e^0\delta)\Phi,$$

$$\text{Constraints} : \left\{(Y^\delta\xi, L_u\xi) \in \mathcal{X} \times \mathcal{F}_u, \quad \forall(\delta, t) \in V_\mathcal{P} \times \widetilde{\Omega}, \right. \tag{29.}$$

where we assume $\delta \in \mathcal{P}$, with $\mathcal{P}$ a convex polytope as in Section 5.4.1. As explicitly shown by Faedo et al. (63), the formulation in Equation 29 always admits a unique solution, due to the linear nature of δ in the associated moment-based equation and the inherent concavity of Equation 19. Furthermore, as in the case of system uncertainty, the unique solution of the robust moment-based WEC formulation for the input uncertainty case is reached precisely at one of the vertices $V_\mathcal{P}$ associated with the corresponding polytope.

5.5. The Case of Wave Energy Converter Arrays

Within the moment-based framework presented in this review, the case of WEC arrays can be dealt with analogously to what has been presented in Section 5, with a suitable redefinition of the associated signal generators. The specific theoretical framework is detailed in References 64 and 65. In brief, each signal generator needs to be augmented by the number of devices in the array N_d accordingly. This can be achieved straightforwardly by replacing each corresponding dynamic matrix S with its augmented counterpart, i.e., with $\mathbb{I}_{N_d} \otimes S$. This naturally implies that the finite-dimensional moment-based programs presented in Sections 5.1 and 5.2 will now be carried over higher-dimensional spaces with respect to their single-device counterparts—i.e., the optimization space is augmented by the number of devices N_d in both cases. Nonetheless, as further clarified in References 64 and 65, this does not affect the main benefits of the moment-based optimal transcription, always admitting a globally optimal energy-maximizing solution, in both linear and nonlinear settings.

6. EXPERIMENTAL IMPLEMENTATION OF MOMENT-BASED CONTROL

This section presents an overview of the experimental implementation and assessment of moment-based control, as described in Section 5 and effectively reported in References 66 and 67. In

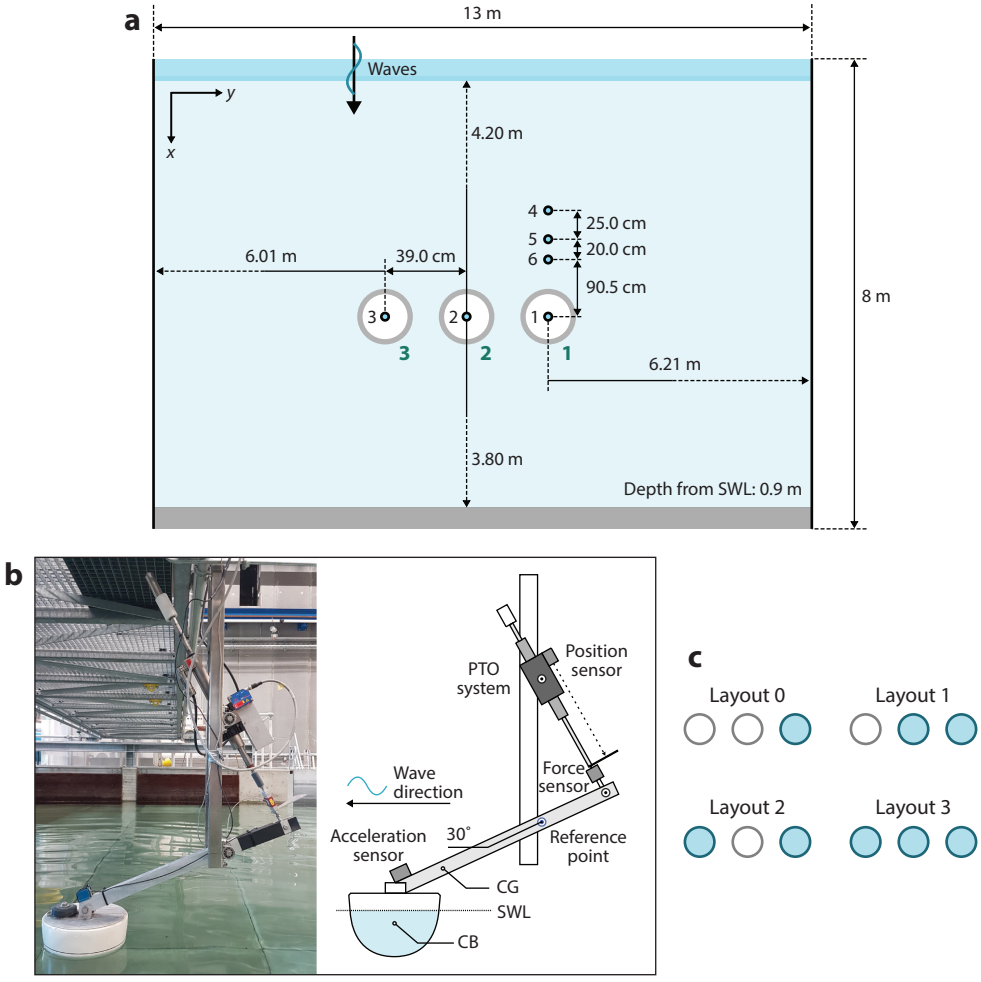

Figure 9

Schematic representation of the wave basin at the Ocean and Coastal Engineering Laboratory at Aalborg University (panel *a*) and an experimental prototype of the Wavestar system (panel *b*). Three prototypes were placed within the wave basin for the experimental campaign, each mounted on a gantry by means of a supporting structure. Four different layout configurations (layouts 0–3; panel *c*) are considered in Reference 67, involving up to three different devices operating simultaneously within the basin. Abbreviations: CB, center of buoyancy; CG, center of gravity; PTO, power take-off; SWL, still water level.

particular, both of those studies considered the same prototype system, described in this section. The main difference is that Reference 66 considered a single prototype, while Reference 67 extended these experimental results by effectively implementing moment-based control for different arrays of WEC systems. Given the larger degree of generalization, this section focuses on the results reported for the array case in Reference 67.

The experimental system considered in Reference 67, illustrated in **Figure 9**, is a small-scale (1:20) prototype of the Wavestar WEC device (68), tested in the basin facilities available at the Ocean and Coastal Engineering Laboratory at Aalborg University, Denmark, as part of a larger experimental campaign in WEC modeling and control executed in September 2022 (69). The system is composed of a floater connected through an arm to a pivoting point fixed in a reference

frame. In the equilibrium position, the arm sits at ∼30° with respect to the horizontal reference frame. The system is free to move in a single DOF and extracts energy from pitch motion (about the reference point; see **Figure 9**) via the attached PTO (linear motor/generator) sitting on the upper structural joint of the device arm (for further detail, see Reference 69). The dimensions of the basin, the placement of the three prototypes, and the four layout configurations considered in Reference 67 are shown in **Figure 9**.

To guarantee operation within the conditions computed via the optimal moment-based algorithm (as described in Section 5.2), the optimal trajectories u^{opt} and y^{opt} are fed to an inner tracking controller, which is in charge of robustly driving the system toward the designed conditions. To achieve this, a proportional–integral–derivative (PID)–like continuous sliding mode controller is used, as developed and proposed by Pérez-Ventura et al. (70). Estimation of the wave excitation force, required for effective implementation of the optimal moment-based reference generation procedure, uses relatively standard techniques, as described by Faedo et al. (66).

Within this experimental campaign, the time horizon T_0 for optimal receding-horizon moment-based trajectory generation (see Section 5.2) is set to 10 s, i.e., a fundamental frequency $\omega_0 \approx 0.63$ rad/s, while the final value for the dimension (order) of the corresponding extended signal generator (as in Equation 20) is $\overline{\nu} = 30$, meaning that 15 harmonics of ω_0 are considered for the construction of $\lambda(\overline{S})$. The moment-based generation sampling rate is set to 25 Hz, i.e., a sampling time $\Delta_h = 0.04$ s, consistent with the experimental studies described by Ringwood et al. (54) and Faedo et al. (66). Constraints are considered for the PTO forces, such that $f_u \in [-12.5, 12.5]$ N·m for each device involved in any particular configuration, according to the specifications for this particular prototype adopted by Ringwood et al. (54). For a detailed account of the tuning rules used within the implementation presented in this section, we direct readers to References 66 and 67.

Figure 10 presents an overview of the experimental performance results obtained within this study, for all the tested layouts and sea states considered, including a comparison with an optimally

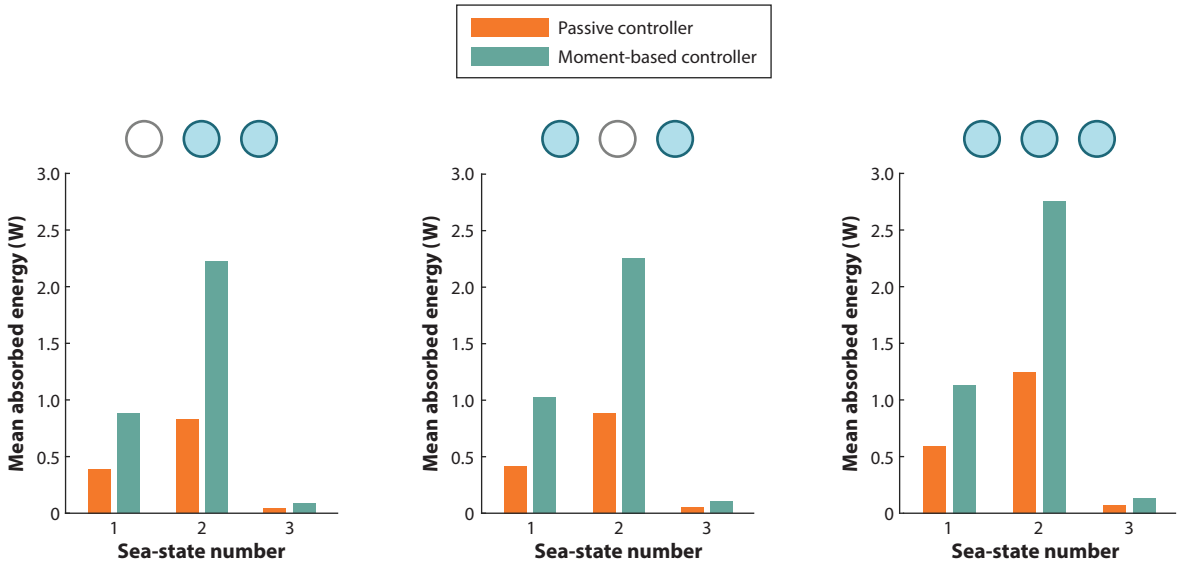

Figure 10

Energy absorbed by each controller for every layout and sea state tested (*top*). The improvement ratio was obtained by considering the moment-based control solution with respect to the benchmark (passive) controller (*bottom*).

tuned benchmark (proportional–passive) controller (see, e.g., 5, 71). In particular, and directly following the control objective in Equation 14, the mean absorbed energy for each full test is considered, taking into account all the devices involved in a given configuration. This is presented explicitly in **Figure 10** for each layout, sea state, and control scenario considered. Note that values of up to ≈2.8 times the energy absorption can be obtained with respect to the benchmark (passive) controller by exploiting moment-based WEC solutions, elucidating the major potential of this framework also in experimental scenarios.

7. CONCLUSIONS

Effective commercialization of wave energy technology inherently requires appropriate control technology that is able to maximize power capture from the wave resource and hence contribute to lowering the associated levelized cost of energy. Nonetheless, the WEC control problem itself does not represent a traditional (stabilization, tracking, or regulation) control objective but rather depends on a suitably defined optimal control formulation, which needs to be solved efficiently in real time. This review offers an overview of moment-based theory as applied to the WEC control problem. We show that this formalism is ideal for solving the WEC control problem, including effective parameterization and model reduction of potentially complex hydrodynamic WEC models. The choice to parameterize the OCP in terms of moments, via a suitably defined signal generator, results in computationally efficient solutions that allow real-time implementation even for arrays of WEC systems, as demonstrated by convincing experimental results. In particular, leveraging tailored approximation methods enables the transition from linear to nonlinear WEC representations—required by the use of the control action itself (which effectively enhances nonlinear behavior when attempting maximization of converted mechanical energy)—to be relatively smooth, presenting, in both cases, guarantees for the existence of globally optimal solutions and hence allowing for the utilization of efficient numerical routines for real-time implementation.

DISCLOSURE STATEMENT

The authors are not aware of any affiliations, memberships, funding, or financial holdings that might be perceived as affecting the objectivity of this review.

ACKNOWLEDGMENTS

The authors are grateful to Professor Alessandro Astolfi and Dr. Giordano Scarciotti of Imperial College London for their input on moment-based theory. This work was supported in part by Science Foundation Ireland under grant 21/FFP-A/8997 and the Marine Renewable Ireland Centre under grant 12/RC/2302-2. This project has received funding from the European Union's Horizon 2020 research and innovation program under Marie Skłodowska-Curie grant agreement 101024372.

LITERATURE CITED

1. Faedo N, Ringwood JV. 2021. A control design framework for wave energy devices. In *Proceedings of the 14th European Wave and Tidal Energy Conference*, pap. 1919. N.p.: Eur. Wave Tidal Energy Conf.
2. Guo B, Ringwood JV. 2021. A review of wave energy technology from a research and commercial perspective. *IET Renew. Power Gen.* 15(14):3065–90
3. Annaswamy AM, Johansson KH, Pappas GJ, eds. 2023. *Control for societal-scale challenges: road map 2030*. Rep., IEEE Control Syst. Soc., Piscataway, NJ
4. Ringwood JV, Zhan S, Faedo N. 2023. Empowering wave energy with control technology: possibilities and pitfalls. *Annu. Rev. Control* 55:18–44

5. Falnes J, Kurniawan A. 2020. *Ocean Waves and Oscillating Systems: Linear Interactions Including Wave-Energy Extraction*. Cambridge, UK: Cambridge Univ. Press
6. Windt C, Faedo N, Penalba M, Dias F, Ringwood JV. 2021. Reactive control of wave energy devices—the modelling paradox. *Appl. Ocean Res.* 109:102574
7. Hals J, Falnes J, Moan T. 2011. Constrained optimal control of a heaving buoy wave-energy converter. *J. Offshore Mech. Arct. Eng.* 133(1):011401
8. Faedo N, Olaya S, Ringwood JV. 2017. Optimal control, MPC and MPC-like algorithms for wave energy systems: an overview. *IFAC J. Syst. Control* 1:37–56
9. Cretel JA, Lightbody G, Thomas GP, Lewis AW. 2011. Maximisation of energy capture by a wave-energy point absorber using model predictive control. *IFAC Proc. Vol.* 44(1):3714–21
10. Astolfi A. 2010. Model reduction by moment matching for linear and nonlinear systems. *IEEE Trans. Autom. Control* 55(10):2321–36
11. Peña-Sanchez Y, Windt C, Davidson J, Ringwood JV. 2019. A critical comparison of excitation force estimators for wave energy devices. *IEEE Trans. Control Syst. Technol.* 28(6):2263–75
12. Peña-Sanchez Y, Garcia-Abril M, Paparella F, Ringwood JV. 2018. Estimation and forecasting of excitation force for arrays of wave energy devices. *IEEE Trans. Sustain. Energy* 9(4):1672–80
13. Cunningham J, Faedo N, Ringwood JV. 2019. Excitation force estimation for wave energy systems using a moment-domain representation. In *Proceedings of the 13th European Wave and Tidal Energy Conference*, pap. 1418. N.p.: Eur. Wave Tidal Energy Conf.
14. Papillon L, Costello R, Ringwood JV. 2020. Boundary element and integral methods in potential flow theory: a review with a focus on wave energy applications. *J. Ocean Eng. Mar. Energy* 6:303–37
15. Ochi MK. 2005. *Ocean Waves: The Stochastic Approach*. Cambridge, UK: Cambridge Univ. Press
16. Babarit A, Delhommeau G. 2015. *Theoretical and numerical aspects of the open source BEM solver NEMOH*. Paper presented at the 11th European Wave and Tidal Energy Conference, Nantes, Fr., Sept. 6–11
17. Lee CH. 1995. *WAMIT theory manual*. Rep., Dep. Ocean Eng., Mass. Inst. Technol., Cambridge, MA
18. Cummins W. 1962. The impulse response function and ship motions. *Schiffstechnik* 47:101–9
19. Folley M, Forehand D. 2016. Conventional multiple degree-of-freedom array models. In *Numerical Modelling of Wave Energy Converters*, ed. M Folley, pp. 151–64. London: Academic
20. Taghipour R, Perez T, Moan T. 2008. Hybrid frequency–time domain models for dynamic response analysis of marine structures. *Ocean Eng.* 35(7):685–705
21. Morison J, Johnson J, Schaaf S. 1950. The force exerted by surface waves on piles. *J. Pet. Technol.* 2(5):149–54
22. Giorgi G, Ringwood JV. 2017. Computationally efficient nonlinear Froude–Krylov force calculations for heaving axisymmetric wave energy point absorbers. *J. Ocean Eng. Mar. Energy* 3:21–33
23. Todalshaug JH, Ásgeirsson GS, Hjálmarsson E, Maillet J, Möller P, et al. 2016. Tank testing of an inherently phase-controlled wave energy converter. *Int. J. Mar. Energy* 15:68–84
24. Richter M, Magaña ME, Sawodny O, Brekken TK. 2013. Nonlinear model predictive control of a point absorber wave energy converter. *IEEE Trans. Sustain. Energy* 4(1):118–26
25. Paduano B, Carapellese F, Pasta E, Faedo N, Mattiazzo G. 2022. Optimal controller tuning for a nonlinear moored wave energy converter via non-parametric frequency-domain techniques. In *Trends in Renewable Energies Offshore*, ed. CG Soares, pp. 393–400. Boca Raton, FL: CRC
26. Gottlieb O, Yim SC. 1992. Nonlinear oscillations, bifurcations and chaos in a multi-point mooring system with a geometric nonlinearity. *Appl. Ocean Res.* 14(4):241–57
27. Narayanan S, Yim S, Polo P. 1998. Nonlinear system identification of a moored structural system. In *The Eighth International Ocean and Polar Engineering Conference*, pap. ISOPE-I-98-264. Richardson, TX: OnePetro
28. Scruggs J, Lattanzio S, Taflanidis A, Cassidy I. 2013. Optimal causal control of a wave energy converter in a random sea. *Appl. Ocean Res.* 42:1–15
29. Faedo N, Scarciotti G, Astolfi A, Ringwood JV. 2018. Energy-maximising control of wave energy converters using a moment-domain representation. *Control Eng. Pract.* 81:85–96
30. Scarciotti G, Astolfi A. 2017. Nonlinear model reduction by moment matching. *Found. Trends Syst. Control* 4(3–4):224–409

31. Astolfi A, Scarciotti G, Simard J, Faedo N, Ringwood JV. 2020. Model reduction by moment matching: beyond linearity a review of the last 10 years. In *2020 59th IEEE Conference on Decision and Control*. Piscataway, NJ: IEEE. **https://doi.org/10.1109/CDC42340.2020.9304389**
32. Isidori A. 1995. *Nonlinear Control Systems*. London: Springer
33. Padoan A, Scarciotti G, Astolfi A. 2017. A geometric characterization of the persistence of excitation condition for the solutions of autonomous systems. *IEEE Trans. Autom. Control* 62(11):5666–77
34. Faedo N, Peña-Sanchez Y, Ringwood JV. 2018. Finite-order hydrodynamic model determination for wave energy applications using moment-matching. *Ocean Eng.* 163:251–63
35. Faedo N, Peña-Sanchez Y, Giorgi G, Ringwood JV. 2019. Moment-matching-based input-output parametric approximation for a multi-DoF WEC including hydrodynamic nonlinearities. In *Proceedings of the 13th European Wave and Tidal Energy Conference*, pap. 1449. N.p.: Eur. Wave Tidal Energy Conf.
36. Faedo N, Peña-Sanchez Y, Ringwood JV. 2019. Parameterisation of radiation forces for a multiple degree-of-freedom wave energy converter using moment-matching. In *The 29th International Ocean and Polar Engineering Conference*, pap. ISOPE-I-19-518. Richardson, TX: OnePetro
37. Faedo N, Peña-Sanchez Y, Ringwood JV. 2020. Parametric representation of arrays of wave energy converters for motion simulation and unknown input estimation: a moment-based approach. *Appl. Ocean Res.* 98:102055
38. Peña-Sanchez Y, Faedo N, Ringwood JV. 2019. A critical comparison between parametric approximation methods for radiation forces in wave energy systems. In *The 29th International Ocean and Polar Engineering Conference*, pap. ISOPE-I-19-521. Richardson, TX: OnePetro
39. Faedo N, Peña-Sanchez Y, Ringwood JV. 2018. Passivity preserving moment-based finite-order hydrodynamic model identification for wave energy applications. In *Advances in Renewable Energies Offshore*, ed. CG Soares, pp. 351–59. Boca Raton, FL: CRC
40. Mekhiche M, Edwards KA. 2014. Ocean Power Technologies Powerbuoy®: system-level design, development and validation methodology. In *Proceedings of the 2nd Marine Energy Technology Symposium*, pp. 1–9. N.p.: Mar. Energy Technol. Symp.
41. Faedo N. 2020. *Optimal control and model reduction for wave energy systems: a moment-based approach*. PhD Thesis, Maynooth Univ., Maynooth, Ireland
42. Faedo N, Dores F, Ringwood JV. 2023. Nonlinear model reduction for wave energy systems: a moment-based approach. *IEEE Trans. Control Syst. Technol.* In press
43. Faedo N, Scarciotti G, Astolfi A, Ringwood JV. 2021. On the approximation of moments for nonlinear systems. *IEEE Trans. Autom. Control* 66(11):5538–45
44. Faedo N, Piuma FJD, Giorgi G, Bracco G, Ringwood JV, Mattiazzo G. 2021. Data-driven nonlinear model reduction by moment-matching for the ISWEC system. In *2021 International Conference on Electrical, Computer, Communications and Mechatronics Engineering*. Piscataway, NJ: IEEE. **https://doi.org/10.1109/ICECCME52200.2021.9591007**
45. Papini G, Piuma FJD, Faedo N, Ringwood JV, Mattiazzo G. 2022. Nonlinear model reduction by moment-matching for a point absorber wave energy conversion system. *J. Mar. Sci. Eng.* 10(5):656
46. Scarciotti G, Jiang ZP, Astolfi A. 2020. Data-driven constrained optimal model reduction. *Eur. J. Control* 53:68–78
47. Ringwood JV, Bacelli G, Fusco F. 2014. Energy-maximizing control of wave-energy converters: the development of control system technology to optimize their operation. *IEEE Control Syst.* 34(5):30–55
48. Mérigaud A, Ringwood JV. 2017. Free-surface time-series generation for wave energy applications. *IEEE J. Ocean. Eng.* 43(1):19–35
49. Boyd SP, Vandenberghe L. 2004. *Convex Optimization*. Cambridge, UK: Cambridge Univ. Press
50. Faedo N, Scarciotti G, Astolfi A, Ringwood JV. 2021. Nonlinear energy-maximizing optimal control of wave energy systems: a moment-based approach. *IEEE Trans. Control Syst. Technol.* 29(6):2533–47
51. Potra FA, Wright SJ. 2000. Interior-point methods. *J. Comp. Appl. Math.* 124(1–2):281–302
52. Faedo N, Giorgi G, Ringwood JV, Mattiazzo G. 2022. Nonlinear moment-based optimal control of wave energy converters with non-ideal power take-off systems. In *Proceedings of the ASME 2022 41st International Conference on Ocean, Offshore and Arctic Engineering*, Vol. 8, *Ocean Renewable Energy*, pap. V008T09A082. New York: Am. Soc. Mech. Eng.

53. Faedo N, Giorgi G, Ringwood JV, Mattiazzo G. 2022. Optimal control of wave energy systems considering nonlinear Froude–Krylov effects: control-oriented modelling and moment-based control. *Nonlinear Dyn.* 109:1777–804
54. Ringwood JV, Ferri F, Tom N, Ruehl K, Faedo N, et al. 2019. The Wave Energy Converter Control Competition: overview. In *Proceedings of the ASME 2019 38th International Conference on Ocean, Offshore and Arctic Engineering*, Vol. 10: *Ocean Renewable Energy*, pap. V010T09A035. New York: Am. Soc. Mech. Eng.
55. Faedo N, Peña-Sanchez Y, Ringwood JV. 2020. Receding-horizon energy-maximising optimal control of wave energy systems based on moments. *IEEE Trans. Sustain. Energy* 12(1):378–86
56. Mosquera F, Faedo N, Evangelista C, Puleston P, Ringwood JV. 2022. Energy-maximising tracking control for a nonlinear heaving point absorber system commanded by second order sliding modes. *IFAC-PapersOnLine* 55(31):357–62
57. Faedo N, Mosquera FD, Evangelista CA, Ringwood JV, Puleston PF. 2022. Preliminary experimental assessment of second-order sliding mode control for wave energy conversion systems. In *2022 Australian & New Zealand Control Conference (ANZCC)*, pp. 63–68. Piscataway, NJ: IEEE
58. Mérigaud A, Tona P. 2020. Spectral control of wave energy converters with non-ideal power take-off systems. *J. Mar. Sci. Eng.* 8(11):851
59. Prabhu KM. 2013. *Window Functions and Their Applications in Signal Processing*. Boca Raton, FL: CRC
60. Faedo N, García-Violini D, Scarciotti G, Astolfi A, Ringwood JV. 2019. Robust moment-based energy-maximising optimal control of wave energy converters. In *2019 IEEE 58th Conference on Decision and Control (CDC)*, pp. 4286–91. Piscataway, NJ: IEEE
61. Ben-Tal A, Nemirovski A. 1998. Robust convex optimization. *Math. Oper. Res.* 23(4):769–805
62. Sniedovich M. 2011. A classical decision theoretic perspective on worst-case analysis. *Appl. Math.* 56(5):499
63. Faedo N, Mattiazzo G, Ringwood JV. 2022. Robust energy-maximising control of wave energy systems under input uncertainty. In *2022 European Control Conference (ECC)*, pp. 614–19. Piscataway, NJ: IEEE
64. Faedo N, Scarciotti G, Astolfi A, Ringwood JV. 2021. Energy-maximising moment-based constrained optimal control of ocean wave energy farms. *IET Renew. Power Gener.* 15(14):3395–408
65. Faedo N, Scarciotti G, Astolfi A, Ringwood JV. 2019. Moment-based constrained optimal control of an array of wave energy converters. In *2019 American Control Conference (ACC)*, pp. 4797–802. Piscataway, NJ: IEEE
66. Faedo N, Peña-Sanchez Y, Garcia-Violini D, Ferri F, Mattiazzo G, Ringwood JV. 2023. Experimental assessment and validation of energy-maximising moment-based optimal control for a prototype wave energy converter. *Control Eng. Pract.* 133:105454
67. Faedo N, Mosquera FD, Pasta E, Papini G, Peña-Sanchez Y, et al. 2023. Experimental assessment of combined sliding mode and moment-based control (SM^2C) for arrays of wave energy conversion systems. *Control Eng. Pract.* In review
68. Hansen RH, Kramer MM. 2011. *Modelling and control of the Wavestar prototype*. Paper presented at the 9th European Wave and Tidal Energy Conference, Southampton, UK
69. Faedo N, Peña-Sanchez Y, Pasta E, Papini G, Mosquera FD, Ferri F. 2023. SWELL: an open-access experimental dataset for arrays of wave energy conversion systems. *Renew. Energt* 212:699–716
70. Pérez-Ventura U, Mendoza-Avila J, Fridman L. 2021. Design of a proportional integral derivative-like continuous sliding mode controller. *Int. J. Robust Nonlinear Control* 31(9):3439–54
71. Carapellese F, Pasta E, Paduano B, Faedo N, Mattiazzo G. 2022. Intuitive LTI energy-maximising control for multi-degree of freedom wave energy converters: the PeWEC case. *Ocean Eng.* 256:111444